Proc. Natl. Acad. Sci. USA
Vol. 94, pp. 8138–8143, July 1997
Medical Sciences

Mouse model of G_{M2} activator deficiency manifests cerebellar pathology and motor impairment

(animal model/G_{M2} gangliosidosis/gene targeting/lysosomal storage disease)

YUJING LIU*, ALEXANDER HOFFMANN†, ALEXANDER GRINBERG‡, HEINER WESTPHAL‡, MICHAEL P. MCDONALD§, KATHERINE M. MILLER§, JACQUELINE N. CRAWLEY§, KONRAD SANDHOFF†, KINUKO SUZUKI¶, AND RICHARD L. PROIA*

*Section on Biochemical Genetics, Genetics and Biochemistry Branch, National Institute of Diabetes and Digestive and Kidney Diseases, ‡Laboratory of Mammalian Genes and Development, National Institute of Child Health and Development, and §Section on Behavioral Neuropharmacology, Experimental Therapeutics Branch, National Institute of Mental Health, National Institutes of Health, Bethesda, MD 20892; †Institut für Oganische Chemie und Biochemie der Universität Bonn, Gerhard-Domagk-Strasse 1, 53121 Bonn, Germany; and ¶Department of Pathology and Laboratory Medicine, and Neuroscience Center, University of North Carolina, Chapel Hill, NC 27599

Communicated by Stuart A. Kornfeld, Washington University School of Medicine, St. Louis, MO, May 12, 1997 (received for review March 21, 1997)

ABSTRACT **The G_{M2} activator deficiency (also known as the AB variant), Tay–Sachs disease, and Sandhoff disease are the major forms of the G_{M2} gangliosidoses, disorders caused by defective degradation of G_{M2} ganglioside. Tay–Sachs and Sandhoff diseases are caused by mutations in the genes (*HEXA* and *HEXB*) encoding the subunits of β-hexosaminidase A. The G_{M2} activator deficiency is caused by mutations in the *GM2A* gene encoding the G_{M2} activator protein. For degradation of G_{M2} ganglioside by β-hexosamindase A, the G_{M2} activator protein must participate by forming a soluble complex with the ganglioside. In each of the disorders, G_{M2} ganglioside and related lipids accumulate to pathologic levels in neuronal lysosomes, resulting in clinically similar disorders with an onset in the first year of life, progressive neurodegeneration, and death by early childhood. We previously have described mouse models of Tay–Sachs (*Hexa* −/−) and Sandhoff (*Hexb* −/−) diseases with vastly different clinical phenotypes. The *Hexa* −/− mice were asymptomatic whereas the *Hexb* −/− mice were severely affected. Through gene disruption in embryonic stem cells we now have established a mouse model of the G_{M2} activator deficiency that manifests an intermediate phenotype. The *Gm2a* −/− mice demonstrated neuronal storage but only in restricted regions of the brain (piriform, entorhinal cortex, amygdala, and hypothalamic nuclei) reminiscent of the asymptomatic Tay–Sachs model mice. However, unlike the Tay–Sachs mice, the *Gm2a* −/− mice displayed significant storage in the cerebellum and defects in balance and coordination. The abnormal ganglioside storage in the *Gm2a* −/− mice consisted of G_{M2} with a low amount of G_{A2}. The results demonstrate that the activator protein is required for G_{M2} degradation and also may indicate a role for the G_{M2} activator in G_{A2} degradation.**

The G_{M2} gangliosidoses are severe neurodegenerative disorders caused by excessive accumulation of G_{M2} ganglioside. Three genetic forms exist: Tay–Sachs disease, Sandhoff disease, and the G_{M2} activator deficiency (also known as the AB variant) (reviewed in ref. 1). Tay–Sachs disease is caused by mutations in the *HEXA* gene, Sandhoff disease by mutations in the *HEXB* gene, and the G_{M2} activator deficiency by mutations in the *GM2A* gene. The *HEXA* and *HEXB* genes encode the α- and β-subunits, respectively, of the lysosomal enzyme, β-hexosaminidase. The subunits dimerize to form the three β-hexosaminidase isozymes, A (αβ), B(ββ), and S (αα). The *GM2A* gene encodes the G_{M2} activator protein. In each disorder, the respective genetic lesion results in impairment of the degradation of G_{M2} ganglioside and related substrates.

In humans, *in vivo* G_{M2} ganglioside degradation requires the G_{M2} activator protein to form a complex with G_{M2} ganglioside. β-Hexosaminidase A then is able to interact with the activator-ganglioside complex and remove the terminal *N*-acetylgalactosamine residue from the oligosaccharide portion of the ganglioside. In both Tay–Sachs and Sandhoff diseases, ganglioside degradation is impaired due to an absence of β-hexosaminidase A. The homodimeric β-hexosaminidase isozymes, S and B, cannot effectively substitute for β-hexosaminidase A in ganglioside degradation. It is believed that the function of the activator protein is to transform the hydrophobic, membrane-bound ganglioside into a substrate complex that is accessible to the water-soluble enzyme (2). Therefore, in the G_{M2} activator deficiency, the ganglioside is refractory to enzymatic hydrolysis by β-hexosaminidase A. In each disease, a massive accumulation of G_{M2} ganglioside and related lipids occurs in neuronal lysosomes, resulting in severe cellular malfunction and damage. The clinical phenotype of each disease is nearly identical. In the most severe forms, the onset of the disease occurs during the first year of life. Rapidly progressing neurodegeneration culminates in demise usually by the age of 4. Disorders of lesser severity and later-onset result when mutations lead to a partial deficiency in ganglioside degradation capacity.

Through targeted gene disruption of the *Hexa* and *Hexb* genes in mouse embryonic stem (ES) cells, we previously have described the creation of mouse models corresponding to Tay–Sachs and Sandhoff diseases (3–5). Unlike the human diseases, the two mouse models were of dramatically different phenotypes as a result of differences in the ganglioside degradation pathway between mice and humans. The Tay–Sachs model developed ganglioside accumulation in restricted regions of the brain but was asymptomatic. The Sandhoff disease model exhibited much more extensive ganglioside accumulation and developed a severe neurologic phenotype.

We now have established mice with a disrupted *Gm2a* gene as a model for the third form of the G_{M2} gangliosidoses. Similar to the *Hexa* −/− mice, the *Gm2a* −/− mice demonstrated storage in restricted regions of the brain. However, these mice also displayed some significant differences. They exhibited storage in the cerebellum, a site of minimal pathology in the *Hexa* −/− mice (4) and developed defects in balance and motor coordination. This mouse model of the G_{M2} activator deficiency is, thus, of an intermediate phenotype when compared with the severely af-

The publication costs of this article were defrayed in part by page charge payment. This article must therefore be hereby marked "*advertisement*" in accordance with 18 U.S.C. §1734 solely to indicate this fact.

Abbreviations: ES, embryonic stem; G_{M1} ganglioside, Galβ1→3GalNAcβ1→4(NeuAcα2→3)Galβ1→4Glcβ1→1Cer; G_{M2} ganglioside, GalNAcβ1→4(NeuAcα2→3)Galβ1→4Glcβ1→1Cer; G_{A2} glycolipid, GalNAcβ1→4Galβ1→4Glcβ1→1Cer; G_{M3} ganglioside, NeuAcα2→3Galβ1→4Glcβ1→1Cer; Cer, ceramide.

fected Sandhoff model and the asymptomatic Tay–Sachs model. The basis for the distinct phenotypes of the human and mouse G_{M2} gangliosidoses are species-specific differences in the ganglioside degradation pathway.

MATERIALS AND METHODS

Targeting Vector Construction. We previously have constructed a plasmid containing both the neomycin-resistance (*neo*) gene and the thymidine kinase gene in the pBluescript KS vector (3). Genomic clones from a 129/SV strain library (Stratagene; catalogue no. 946306) containing the mouse *Gm2a* gene were isolated and characterized. A 4.5-kb genomic fragment containing part of intron 2 was inserted between the *Sal*I and *Not*I sites downstream of the *Neo* gene. Next, a 4.5-kb genomic fragment containing part of the exon 4 and downstream region was cloned into the *Xho*I site between the thymidine kinase and *Neo* genes. The organization of the targeting vector is illustrated in Fig. 1*A*. The design of the targeting vector would result in a 1-kb deletion that includes the entire exon 3, entire intron 3, and part of exon 4.

Selection of Targeted ES Cells and Generation of Mutant Mice. The targeting vector (50 μg) was linearized with *Ssp*I endonuclease and introduced into the J1 line (6) of ES cells (1.6×10^7 cells) by electroporation (400 V and 25 μF) in a Bio-Rad Gene Pulser. Targeted clones were isolated as described (3). Targeted ES cells lines Act-4 and Act-25 were injected into the blastocysts of 3.5-day C57BL/6 embryos. Highly chimeric male mice were obtained and bred to C57BL/6 females. The agouti

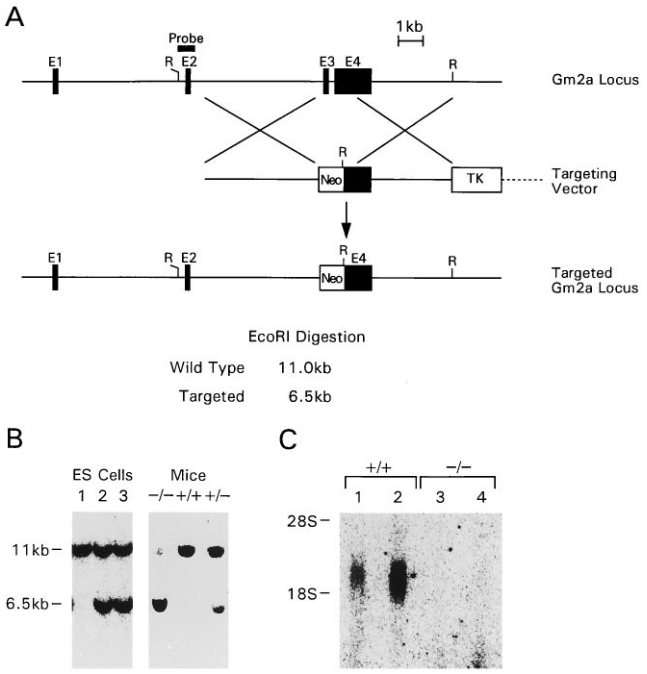

FIG. 1. Targeted disruption of the *Gm2a* locus. (*A*) The mouse *Gm2a* locus is indicated on top, the structure of the mouse *Gm2a* targeting vector is in the middle, and the predicted structure of the homologously recombined locus is on the bottom. R, *Eco*RI site; TK, thymidine kinase gene, E, exon. (*B*) Southern analysis of ES clone and mouse tail DNA. Genomic DNA was isolated, digested with *Eco*RI endonuclease, electrophoresed on a 1% agarose gel, and transferred to GeneScreen*Plus* membranes. The hybridization probe is shown in *A*. (*Left*) Lane 1 shows a G418-resistant clone that had not undergone homologous recombination. Lanes 2 and 3 show correctly targeted clones. (*Right*) Tail DNA from *Gm2a* −/−, +/+, and +/− mice. (*C*) Northern analysis of testis and kidney from *Gm2a* +/+ and −/− mice. Twenty micrograms of total RNA from testis or kidney RNA was subjected to electrophoresis through a 1.2% formaldehyde/agarose gel, transferred to GeneScreen*Plus* membrane, and hybridized with *Gm2a* cDNA probe. Lanes 1 and 3, testis; lanes 2 and 4, kidney.

offspring were tested for transmission of the disrupted allele by Southern blot analysis. Heterozygous matings were set up to generate homozygous mutant mice.

Biochemical Analysis. β-Hexosaminidase assays were performed as described (3). Methodology for the analysis of brain lipids from gray and white matter has been described (5).

Pathology. Six *Gm2a* −/− and two *Gm2a* +/− mice, ages ranging from 2 to 7 months, were studied. Mice were anesthetized and perfused with phosphate-buffered 4% paraformaldehyde (pH 7.4). The brain, spinal cord, and pieces of visceral organs from two of the *Gm2a* −/− mice were processed for paraffin sections, cut and stained with hematoxylin-eosin, solochrome-eosin, Luxol-fast blue-periodic acid-Schiff, and Bielschowsky stains. In other mice the cerebrum, cerebellum, brainstem, and spinal cord were cryoprotected by immersion in 0.1 M phosphate buffer (pH 7.4) containing 30% sucrose, snap-frozen in a Hist Bath (Shandon, Pittsburgh), and serially sectioned at 7 μm thick with a Frigocut 2800 (Leica, Germany). Every fourth section was stained with periodic acid-Schiff and counter-stained lightly with hematoxylin.

Behavioral Methods. Subjects were 24 mice (six wild type, six *Gm2a* +/−, and 12 *Gm2a* −/−). All procedures were approved by the National Institute of Mental Health Animal Care and Use Committee and followed the National Institutes of Health guidelines, "Using Animals in Intramural Research." Mice were 13 weeks old at the start of testing. Body weights were measured biweekly during the 20-week testing period. There were no significant differences in body weight across treatment groups. Male mice weighed significantly more than females across all groups ($F_{1,18} = 32.59$, $P < 0.0001$). Repeated-measures analysis showed that there was a significant increase in weight over the 20-week testing period across all groups combined ($F_{9,162} = 83.61$, $P < 0.0001$), but no difference in weight gain among groups.

Rotorod. The ability to maintain balance on a rotating cylinder was measured with a standard rotorod apparatus (model 7650, Ugo Basile, Varese, Italy). The cylinder was 3.2 cm in diameter and covered with textured rubber. Mice were confined to a section of the cylinder 6.0 cm long by gray Plexiglas dividers. Each mouse was placed on the cylinder, which increased rotation speed over a 5-min period from 5 to 40 revolutions per min. Rotational speed at which the mouse fell off the rotating cylinder was measured. Mice that fell in less than 15 s were given a second trial. Mice that did not fall during the 300-s trial period were removed and given a score of 40 rpm. Rotorod testing was conducted once every 2 weeks for 20 weeks.

Open field behavior. Exploratory locomotor activity was measured in an open field as described (3, 5). Locomotor activity was measured once every 2 weeks for 20 weeks.

Passive avoidance. Passive avoidance learning was tested in a mouse shuttle box as described (3, 5).

Shock threshold. Testing was performed as described (7).

Tail-flick nociception. Each mouse was placed within a restraining tube on a tail-flick monitor (Omnitech Electronics, Columbus, Ohio). The mouse's tail protruded from a hole in the restraining tube and was allowed to move freely. The mouse's tail was placed in a tail guide, which contained a photobeam for precise measurement of tail-flick latencies. A coil, offset in the floor of the monitor, was used to apply a heat stimulus to the mouse's tail. The temperature of the heating coil rose 15.0°C from room temperature in 15 s. The time it took for the mouse to flick its tail away from the heat was measured automatically by completing the photobeam upon tail flick.

Hot-plate nociception. Each mouse was placed on a hot plate maintained at 55°C (Nuova II; Thermolyne, Dubuque, Iowa). A plastic cylinder 15 cm in diameter and 12.5 cm high confined the mouse to the surface of the hot plate. The time it took the mouse to jump or lick its paw was measured with a stop watch. Mice were then immediately removed from the hot plate. Mice that did not jump or lick a paw within 10 s were removed from the hot plate and given a score of 10 s.

Startle response/prepulse inhibition. Startle response and prepulse inhibition were measured using two SR-Lab startle chambers (San Diego Instruments, San Diego, CA). Each chamber contained a Plexiglas cylinder 5.1 cm in diameter, resting on a Plexiglas frame (20.4 cm length × 12.7 cm width × 0.4 cm thick) within a ventilated enclosure. The startle session was immediately preceded by a 5-min acclimation period in the startle chambers. The mice were then tested with a series of white noise bursts in the chamber, presented through a loudspeaker mounted 28 cm above the animal. Each startle session consisted of 42 trials over a 10.5-min period. There were seven trial types: six trials on which no stimulus was presented, six trials on which only the startle stimulus was presented, and 30 trials on which the startle stimulus was preceded by one of five "prepulse" stimuli, by 100 ms. The startle stimulus was a 40-ms, 120-dB burst of white noise. The prepulse stimuli were 20-ms bursts of 74, 78, 82, 86, or 90-dB white noise, each presented on six trials. The trials on which no stimulus was presented were used to measure baseline movement in the cylinders. The seven trial types were presented in pseudorandom order such that each trial type was presented once within a block of seven trials. The intertrial interval ranged from 10–20 s with an average of 15 s. The startle response was recorded for 65 ms (sampling the response once every 1 ms), starting with the onset of the startle stimulus. The maximal startle amplitude recorded during the 65-ms sampling window was used as the dependent variable.

Statistical analysis. Because there were no differences on any measure between wild types and heterozygotes, these two groups were combined into a single control group for statistical analysis. Two-group comparisons were made using unpaired Student's *t* tests. Analyses of performance over time were made using two-factor repeated-measures ANOVA.

RESULTS

Targeted Disruption of the Mouse *Gm2a* Gene. Using a mouse *Gm2a* cDNA (8) as probe, we isolated genomic DNA fragments covering the entire mouse *Gm2a* gene from a 129/sv strain library. Like the human *GM2A* gene (9), the mouse *Gm2a* gene has four exons (Fig. 1*A*). The exon-intron borders are completely conserved between human and mouse (Y.L. and R.L.P., unpublished results).

To disrupt the *Gm2a* gene in mouse ES cells, a replacement-type of targeting vector was created with these genomic segments. A 1-kb region covering exon 3 and the entire coding region of exon 4 was deleted and replaced with the MC1NeopolyA cassette. The targeting vector had a total of 9 kb of homologous genomic sequence with 4.5 kb of sequence flanking each side of the Neo cassette. Additionally, the thymidine kinase gene was positioned outside the homologous sequences to enable selection against nonhomologous integrants.

The targeting vector was linearized and electroporated into the J1 ES cell line. The ganciclovir counter selection resulted in a 7-fold enrichment of homologous recombinants. Genomic DNA from G418- and ganciclovir-resistant clones was analyzed by Southern analysis. Of the 113 colonies examined, DNA from 13 contained the 6.5-kb *Eco*RI band diagnostic of a homologous recombination event (Fig. 1*B*). Cells from two of the targeted ES clones were injected into C57BL/6 mouse blastocysts, and one of the clones produced highly chimeric male mice that transmitted the targeted allele through the germ line. The heterozygotes were intercrossed to obtain mice homozygous for the disrupted gene (Fig. 1*B*).

The *Gm2a* Homozygous Mutant Mouse Has a Total G_{M2} Activator Deficiency with Normal Hexosaminidase Activity. The targeting event resulted in a deletion of the C-terminal 112 amino acids of the 162 total amino acids contained within the mature G_{M2} activator protein. The deletion was evidenced by genomic Southern blot analysis using a cDNA probe composed of the coding sequence presumed removed during homologous recombination. With this probe, no hybridization signal was detected from the homozygous mutant mice (data not shown). The total RNA of testis and kidney from wild-type and *Gm2a* −/− mice was examined by Northern blot analysis (Fig. 1*C*). A ≈2.3-kb mRNA was detected in wild-type mice tissues. No *Gm2a*-related transcript was present in the *Gm2a* −/− mice tissues, demonstrating that the targeting event resulted in a null allele.

Like humans with G_{M2} activator deficiency, the *Gm2a* −/− mice had normal levels of β-hexosaminidase activity. Liver extracts from wild-type, *Hexa* −/−, *Hexb* −/−, and *Gm2a* −/− were chromatographed on a Mono Q column under conditions that separate β-hexosaminidase A and B (3). Different from the *Hexa* −/− and *Hexb* −/− mice that lacked one or both of the two isozymes, the *Gm2a* −/− mice had normal levels of β-hexosaminidase isozyme activity (data not shown)

Glycolipid Accumulation in *Gm2a* −/− Mice. Sphingolipids were isolated from gray matter and white matter of brains from wild-type, *Hexa* −/−, *Hexb* −/−, and *Gm2a* −/− mice at 4 months of age. The glycolipid fraction was then separated by high-performance thin-layer chromatography, and the G_{M2} and G_{A2} species were quantified (Fig. 2). The *Gm2a* −/− mice accumulated G_{M2} ganglioside in their brains at a level comparable to the *Hexa* −/− mice but less than the *Hexb* −/− mice. As previously described (5) the *Hexb* −/− mice also accumulated a large amount of G_{A2}. The *Gm2a* −/− mice did not accumulate large amounts of G_{A2}. However, a closely migrating band made it difficult to determine if a small amount of G_{A2} was present in the *Gm2a* −/− mice by this analysis.

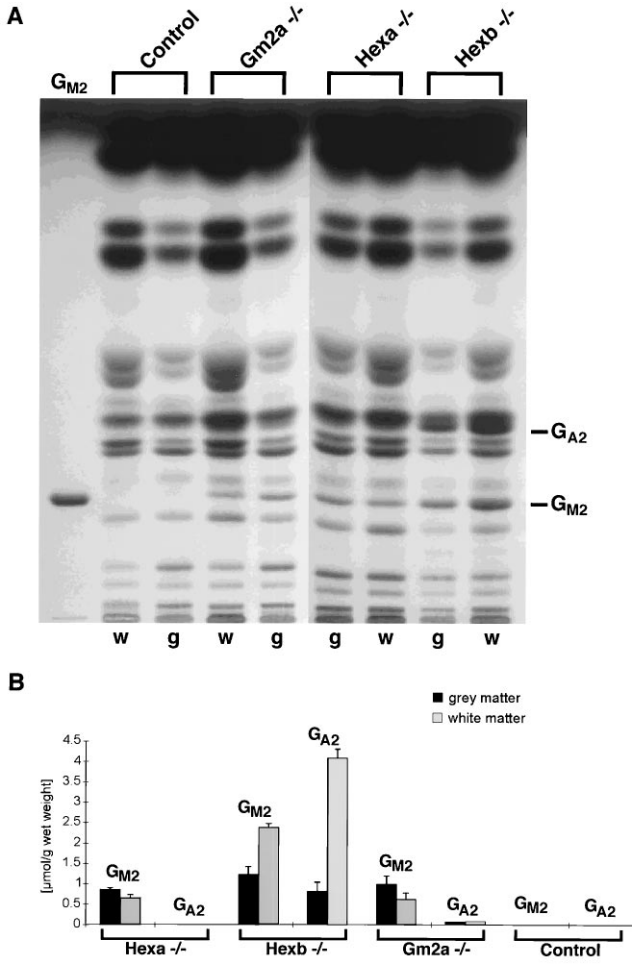

FIG. 2. Glycolipid accumulation in the brains of 4-month-old *Hexa* −/−, *Hexb* −/−, and *Gm2a* −/− mice. (*A*) The sphingolipid fraction of brain tissues was separated by thin-layer chromatography. G_{M2} and G_{A2} standards are indicated. g, gray matter; w, white matter. (*B*) The sphingolipid fraction of gray and white matter was quantified, respectively (μmol/g wet weight).

Therefore the gray and white matter glycolipids were separated in a two-dimensional high-performance thin-layer chromatography system (first solvent: $CHCl_3$/MeOH/7 M NH_4OH (65:25:4 vol/vol), second solvent system: $CHCl_3$/MeOH/H_2O, 0.22% $CaCl_2$ (60:35:8 vol/vol). In this analysis, a heavy G_{A2} accumulation was found in *Hexb* −/− mice, no G_{A2} was detected in *Hexa* −/− mice and, most importantly, a slight accumulation was identified in the *Gm2a* −/− mice.

The ganglioside degradation pathway of the *Gm2a* −/− mice was analyzed by administration of G_{M1} ganglioside radiolabled in the ceramide moiety to cultured embryonic fibroblasts (Fig. 3). As a result of the absence of both β-hexosaminidase A and B, the fibroblasts from *Hexb* −/− and from double-knockout (*Hexa* −/− and *Hexb* −/−) mice could only degrade G_{M1} to G_{M2} and G_{A2} (5, 10). As described previously, *Hexa* −/− fibroblasts bypassed this block as a result of sialidase action on G_{M2} to produce G_{A2} and the subsequent degradation of G_{A2} by β-hexosaminidase B (5). Like the *Hexa* −/− fibroblasts, but distinct from the *Hexb* −/− fibroblasts, the *Gm2a* −/− fibroblasts also degraded G_{M1} to ceramide, demonstrating that the catabolic pathway in these mice was not completely blocked. However, the *Gm2a* −/− fibroblasts accumulated a higher quantity of G_{A2} than that found in the *Hexa* −/− fibroblasts.

***Gm2a* −/− Mice Show Restricted Neuronal Storage.** *Gm2a* −/− mice aged 2 to 7 months were examined. Although the central nervous system pathology progressively worsened with age, the overall distribution of the pathology was the same regardless of the age of the animal. Unless noted otherwise, the description here is given for 5-month-old mice. Examination was carried out using periodic acid-Schiff staining on frozen sections, which results in the ganglioside storage appearing red. As previously described, the *Hexa* −/− mice showed a pattern of storage restricted to certain regions of the brain whereas the *Hexb* −/− mice exhibited storage throughout the brain. In the cerebral cortex, the pattern of neuronal storage in *Gm2a* −/− mice was very similar to that of the *Hexa* −/− mice (4). The storage was predominately in large pyramidal neurons in the middle layer (Fig. 4 *A* and *B*). In contrast, almost all neurons in the cerebral cortex from the *Hexb* −/− mice contained storage material (Fig. 4*C*). Also like the *Hexa* −/− mice (4), storage in the *Gm2a* −/− mice was most pronounced in certain areas such as in the piriform, entorhinal cortex, and amygdala as well in the hypothalamic nuclei (data not shown). In both the *Gm2a* −/− and *Hexa* −/− mice little storage was observed in spinal cord and visceral organs (refs. 4 and 5; data not shown).

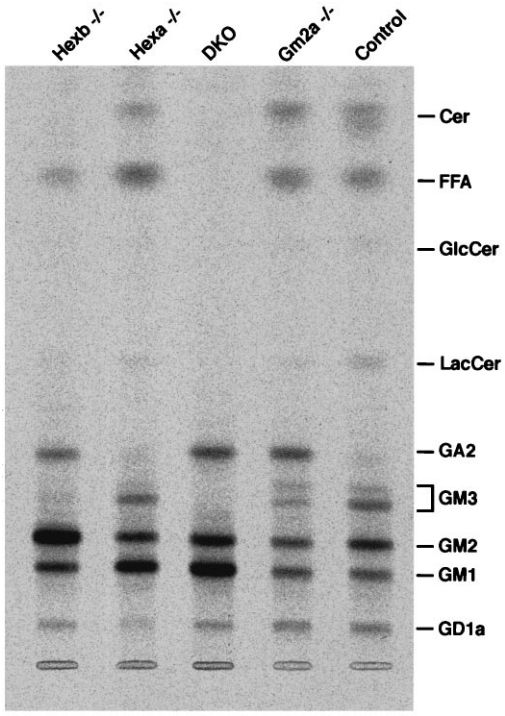

FIG. 3. Ganglioside metabolism in gangliosidosis fibroblasts. [^{3}H]G_{M1} ganglioside was added to fibroblast cultures for 120 hr. The glycolipids then were extracted, analyzed by thin-layer chromatography and visualized on a Raytest/Fuji BAS 1000 phosphoimager. (*Left to right*) *Hexb* −/−, *Hexa* −/−, DKO (double knockout, both *Hexa* −/− and *Hexb* −/−), *Gm2a* −/−, and control (wild-type) embryonic fibroblasts. Cer, ceramide; FFA, free fatty acid; GlcCer, glucosylceramide; LacCer, lactosylceramide.

The major difference between the neuropathology of the *Gm2a* −/− and *Hexa* −/− mice was the presence of storage cells in the cerebellum in the former. In *Gm2a* −/− mice, prominent storage material was present in the glial cells in the molecular and granular cell layers, and Purkinje and granular cell neurons (Fig. 4 *D* and *E*). A similar distribution of cerebellar storage also was observed in the youngest *Gm2a* −/− mice examined (2 months old). Very little storage was observed in comparable areas of the *Hexa* −/− cerebellum at any age. In the *Hexb* −/− mice, storage was abundant in the Purkinje cells as well as in the granular cells and molecular layer of the cerebellum (Fig. 4*F*).

***Gm2a* −/− Mice Are Viable but Have Neurologic Disturbances.** Heterozygous matings yield *Gm2a* −/− progeny in a Mendelian fashion, indicating that there was no embryonic lethality. *Gm2a* −/− mice grow normally and have survived for more than 1 year. Both males and females are fertile. They can be bred to each other and give litters of normal size.

The *Gm2a* −/− mice were tested to determine their neurologic function. Motor coordination and balance was measured with a standard rotorod apparatus. A total of 24 mice (six wild type, six *Gm2a* +/−, and 12 *Gm2a* −/−) were tested beginning at 13 and ending at 31 weeks of age. As shown in Fig. 5*A*, overall rotorod performance was significantly impaired in the knockouts, compared with the controls ($F_{1,22} = 5.18$, $P = 0.033$). Analysis of the groups individually demonstrated that the controls displayed a significant improvement in rotorod performance over the 20-week testing period ($F_{9,99} = 4.36$, $P < .0001$), while the performance of the knockouts remained stable ($F_{9,99} = 0.89$, $P = 0.534$). Using open field testing, there was no significant difference between *Gm2a* −/− and controls in horizontal activity ($F_{1,22} = 3.99$, $P = 0.058$) or vertical activity ($F_{1,22} = 0.215$, $P = 0.647$), indicating the poor performance of the *Gm2a* −/− mice on the rotorod was not due to a generalized lack of mobility.

The passive-avoidance task was used as a test for learning and memory. Fig. 5*B* illustrates passive-avoidance performance on the training and testing days for *Gm2a* −/− and control mice. There was no difference between groups on latency to enter the dark chamber on the training trial ($t20 = 0.20$, $P = 0.657$). However, there was a small, but significant, difference in latency to enter the dark chamber 24 hr after a foot shock in that location ($t20 = 2.42$, $P = 0.025$), indicating a possible memory deficit in the *Gm2a* −/− mice. No significant differences were detected among genotypes with the shock threshold test or with the tail-flick and hot-plate tests for nociception, suggesting that the deficit in passive-avoidance learning was not due to shock or pain insensitivity. No significant differences were detected among genotypes on prepulse inhibition, indicating that sensorimotor gating was normal in the *Gm2a* −/− mice.

DISCUSSION

We have established mouse models for the three major forms of the G_{M2} gangliosidoses: Tay–Sachs disease, Sandhoff disease, and, as described here, the G_{M2} activator deficiency (AB variant). Although the three human disorders are very similar in clinical phenotype, each of the mouse models displays a distinct phenotype. The Sandhoff mice (*Hexb* −/−), lacking β-hexosaminidase A and B, are the most severely affected with an early onset of severe, progressing motor dysfunction and a shortened life span. In contrast, the Tay–Sachs mice (*Hexa*

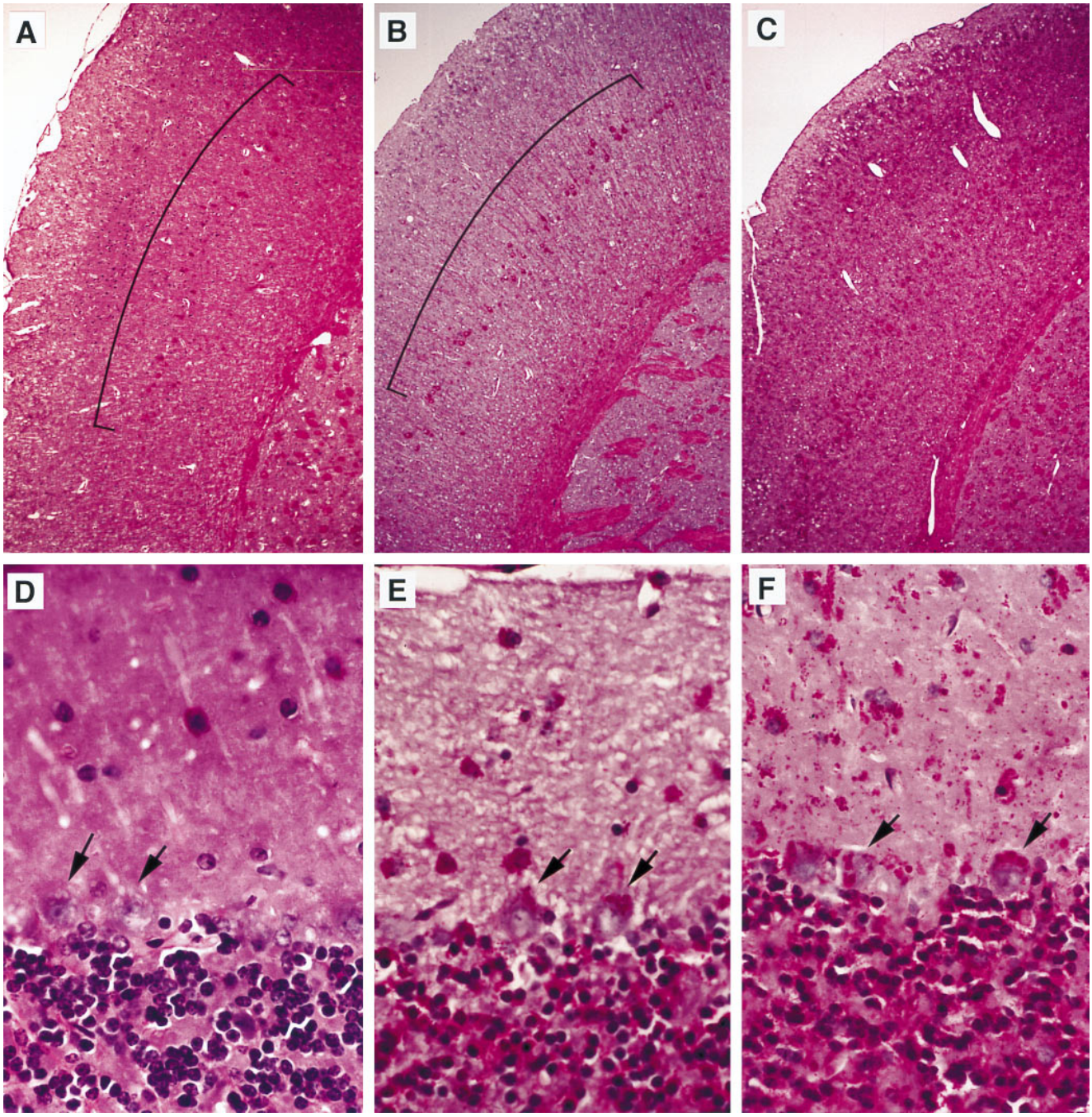

FIG. 4. *Gm2a* −/− and *Hexa* −/− mice show restricted storage in the brain compared with *Hexb* −/− mice. All panels are photomicrographs of frozen sections stained by periodic acid-Schiff. *B* displays cerebral cortex from the *Gm2a* −/− mouse with storage predominant in large pyramidal neurons in the middle layer (bracketed) similar to the *Hexa* −/− mouse in *A*; while nearly all neurons contain storage in the *Hexb* −/− mouse (*C*). (×30.) (*E*) The cerebellum of the *Gm2a* −/− mouse shows storage in some Purkinje cells (arrows), glial cells in the molecular cell layer, and some granular cell neurons (may be also glial cells) in the granular cell layers. (*D*) In a similar section from a *Hexa* −/− mouse minimal storage is seen in a few glial cells in the molecular layer but not in Purkinje cells (arrows). (*F*) The *Hexb* −/− mouse shows more storage in Purkinje cells (arrows), granular cells, and molecular layer. (×300.)

−/−), lacking β-hexosaminidase A, appear to be phenotypically normal. The *Gm2a* −/− mice, which do not express the activator protein, are of an intermediate phenotype with motor function abnormalities but with a normal life span.

The basis for the phenotypic differences between the human and mouse gangliosidoses is in large measure the result of different degradative pathways. Based on the biochemical differences between the *Hexa* −/− and *Hexb* −/− mice, we have proposed two independent catabolic pathways for G_{M2} in mice (5). In one, G_{M2} is degraded to G_{M3} primarily by β-hexosaminidase A with the G_{M2} activator protein. This is the major and almost exclusive pathway in humans. In a second pathway specific to the mouse, G_{M2} is degraded by sialidase first to G_{A2} and then by β-hexosaminidase B or A to lactosylceramide (Fig. 6). Consequently, the *Hexa* −/− mice lacking β-hexosaminidase A accumulate G_{M2}, but not G_{A2}, and are asymptomatic. The *Hexb* −/− mice lacking both β-hexosamindase A and B accumulate *both* G_{M2} and G_{A2} due to blocks in both pathways and show a severe phenotype. In the brain of the *Gm2a* −/− mice there is accumulation of G_{M2} with a small amount of G_{A2}. The G_{M2} accumulation proves that the activator protein is essential for the degradation of G_{M2} ganglioside via the formation of G_{M3} and

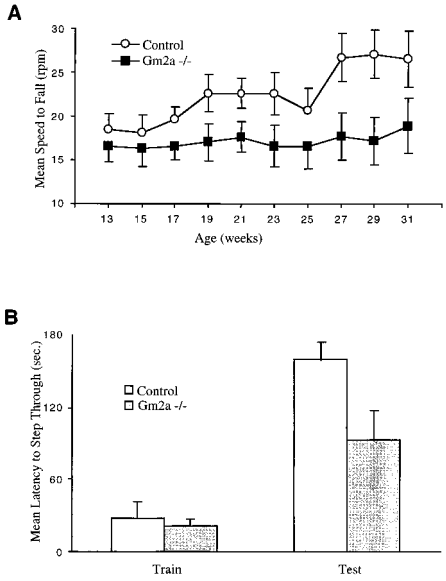

FIG. 5. *Gm2a* −/− mice show difference in motor coordination and possible memory deficit when compared with control mice. (*A*) The ability to maintain balance on a rotating rotorod was measured every 2 weeks beginning at 13 weeks of age. Mean (±SEM) speed to fall from the rotorod for *Gm2a* −/− (n = 12) and controls (n = 12). Controls stayed on the rotorod significantly longer than *Gm2a* −/− mice overall. Controls exhibited improved rotorod performance over the 20-week testing period, while performance of the *Gm2a* −/− mice remained stable. (*B*) Mean (±SEM) latency to enter a dark chamber on the passive avoidance task for *Gm2a* −/− (n = 10) and controls (n = 12). *Gm2a* −/− mice were quicker to enter the dark chamber on the test trial, indicating poorer retention for the aversive experience of the previous day.

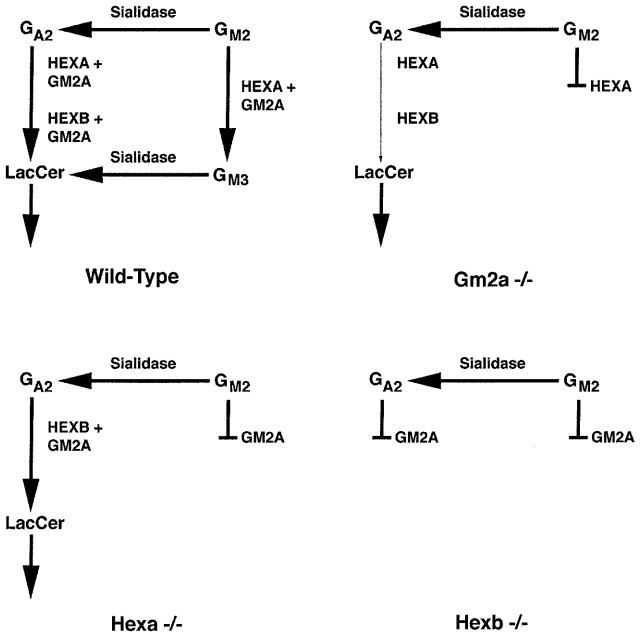

FIG. 6. The ganglioside degradation pathways in gangliosidosis mice. The normal degradative pathway in mice has been described (5). Also shown are proposed degradative pathways in *Hexa* −/−, *Hexb* −/−, and *Gm2a* −/− mice. This scheme does not take into account the minor contribution of β-hexosaminidase S on G_{M2} hydrolysis. G_{M2}, G_{M2} ganglioside; G_{M3}, G_{M3} ganglioside; G_{A2}, G_{A2} glycolipid; LacCer, lactosylceramide; HEXA, β-hexosaminidase A; HEXB, β-hexosaminidase B; GM2A, G_{M2} activator protein.

demonstrates, together with the results from the *Hexa* −/− mice, that both the activator protein and β-hexosaminidase A are needed for this reaction in mice as in humans (Fig. 6).

The low level of G_{A2} storage in the *Gm2a* −/− mice indicates that the hexosaminidase-mediated degradation of G_{A2} can proceed in the absence of the activator protein. However, evidence also suggests that the activator protein is likely required for this reaction to proceed at an optimal rate. In the ganglioside feeding experiment *Gm2a* −/− fibroblasts contained a higher quantity G_{A2} than *Hexa* −/− or wild-type fibroblasts. This result is consistent with the G_{M2} activator protein increasing the rate of G_{A2} degradation by hexosaminidase A and/or B. Indeed, administration of recombinant human G_{M2} activator protein to mouse *Gm2a* −/− fibroblasts enhances the degradation of radiolabled G_{A2} (A.H. and K. Sandhoff, unpublished results).

The pathologic differences between the *Hexa* −/− and *Gm2a* −/− mice also indicate that ganglioside catabolism pathway is not equivalent in the two types of mice. For the most part, the regions of the brain affected by storage were very similar in the two knockout mice indicative of a common degradative block at G_{M2} to G_{M3} (Fig. 6). A major difference between the *Gm2a* −/− and the *Hexa* −/− mice was the presence of storage in the cerebellar neurons and glial cells of the *Gm2a* −/− mice. The impaired motor coordination detected in the *Gm2a* −/− mice was consistent with significant storage in this portion of the brain. With minimal storage in this cerebellar region, the *Hexa* −/− mice were asymptomatic throughout their normal life span. Cerebellar storage in the *Gm2a* −/−, but not the *Hexa* −/−, mice must be due to the inability of the activator-independent degradative pathway to handle the level of ganglioside substrate produced in this region of the brain. This accumulation in the *Gm2a* −/− cerebellum could be explained by a lower rate of G_{A2} degradation in the absence of activator relative to when activator is present in the *Hexa* −/− cerebellum. As illustrated by the late-onset forms of the G_{M2} gangliosidoses, very low levels of degrading activity can drastically alter the degree of ganglioside storage (11, 12).

The three gangliosidosis mice provide models for the human disorders, allowing evaluation of potential therapies including protein and gene replacement, stem cell transplantation, and substrate depravation strategies (13). In addition, the degradative pathways in the mildly affected mice suggest possible therapies through manipulation of the human degradative pathway.

We thank Raymond Thertulien for help with the isolation of the mouse *Gm2a* −/− genomic clones. This work was supported in part by U.S. Public Health Service Grants RO1-NS 24453 and P30-HD 03110 and the Deutsche Forschungsgemeinschaft (SFB 284).

1. Gravel, R. A., Clarke, J. T. R., Kaback, M. M., Mahuran, D., Sandhoff, K. & Suzuki, K. (1995) in *The Metabolic and Molecular Basis of Inherited Disease*, eds. Scriver, C. R., Beaudet, A. L., Sly, W. S. & Valle, D. (McGraw-Hill, New York), pp. 2839–2879.
2. Sandhoff, K. & Kolter, T. (1996) *Trends Cell Biol.* **6,** 98–103.
3. Yamanaka, S., Johnson, M. D., Grinberg, A., Westphal, H., Crawley, J. N., Taniike, M., Suzuki, K. & Proia, R. L. (1994) *Proc. Natl. Acad. Sci. USA* **91,** 9975–9979.
4. Taniike, M., Yamanaka, S., Proia, R. L., Langaman, C., Bone-Turentine, T. & Suzuki, K. (1995) *Acta Neuropathol.* **89,** 296–304.
5. Sango, K., Yamanaka, S., Hoffmann, A., Okuda, Y., Grinberg, A., Westphal, H., McDonald, M. P., Crawley, J. N., Sandhoff, K., Suzuki, K. & Proia, R. L. (1995) *Nat. Genet.* **11,** 170–176.
6. Lee, K.-F., Li, E., Huber, J., Landis, S. C., Sharpe, A. H., Chao, M. V. & Jaenisch, R. (1992) *Cell* **69,** 737–749.
7. Bourtchuladze, R., Frenguelli, B., Blendy, J., Cioffi, D., Schutz, G. & Silva, A. J. (1994) *Cell* **79,** 59–68.
8. Yamanaka, S., Johnson, O. N., Lyu, M. S., Kozak, C. A. & Proia, R. L. (1994) *Genomics* **24,** 601–604.
9. Klima, H., Tanaka, A., Schnabel, D., Nakano, T., Schoder, M., Suzuki, K. & Sandhoff, K. (1991) *FEBS Lett.* **289,** 260–264.
10. Sango, K., McDonald, M. P., Crawley, J. N., Mack, M. L., Tifft, C. J., Skop, E., Starr, C. M., Hoffmann, A., Sandhoff, K., Suzuki, K. & Proia, R. L. (1996) *Nat. Genet.* **14,** 348–352.
11. Conzelmann, E. & Sandhoff, K. (1991) *Dev. Neurosci.* **13,** 197–204.
12. Leinekugel, P., Michel, S., Conzelmann, E. & Sandhoff, K. (1992) *Hum. Genet.* **88,** 513–523.
13. Platt, F. M., Neises, G. R., Reinkensmeier, G., Townsend, M. J., Perry, H. V., Proia, R. L., Winchester, B., Dwek, R. A. & Butters, T. D. (1997) *Science* **276,** 428–431.